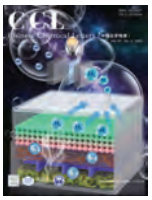
Chinese Chemical Letters 37 (2026) 111516

Contents lists available at ScienceDirect

Chinese Chemical Letters

journal homepage: www.elsevier.com/locate/cclet



Sequential FRET system based on macrocyclic AIEgens for versatile photocatalysis

Meng-Xin Liu[a], Xiao-Long Su[a,*], Pu Chen[a], Yan-Yan Liu[a], Jian-Peng Li[a], Li Zou[a], Ben Zhong Tang[b,*], Hai-Tao Feng[a,*]

[a] AIE Research Center, Shaanxi Key Laboratory of Phytochemistry, College of Chemistry and Chemical Engineering, Baoji University of Arts and Sciences, Baoji 721013, China

[b] Guangdong Basic Research Center of Excellence for Aggregate Science, School of Science and Engineering, Shenzhen Institute of Aggregate Science and Technology, The Chinese University of Hong Kong, Shenzhen (CUHK-Shenzhen), Shenzhen 518172, China

ARTICLE INFO

Article history:
Received 22 April 2025
Revised 23 June 2025
Accepted 25 June 2025
Available online 26 June 2025

Keywords:
Macrocycles
AIEgens
Light-harvesting systems
Sequential energy transfer
Photocatalysis

ABSTRACT

Supramolecular architectures exhibiting cascade energy transfer characteristics represent pivotal model systems for advancing biomimetic light-harvesting systems (LHS) that emulate the natural photosynthesis. To now, the engineering of aqueous-phase artificial LHS with optimized energy transfer cascades is still a challenge. In this study, we designed and synthesized two tetraphenylethylene (TPE)-based macrocyclic compounds (namely TPE-1 and TPE-2) with different cavity sizes as supramolecular scaffolds to study their energy transfer behaviors. As a control model, a linear molecule TPE-3 was also prepared. The bigger-cavity macrocycle TPE-1 can emit green fluorescence and self-assemble into nanospherical structures in aqueous media, acting as an energy donor. Through self-assembly with eosin Y (EY) and a red-emitting fluorophore (TPE-Se), a sequential Förster resonance energy transfer (FRET) cascade: TPE-1→EY→TPE-Se was achieved thanks to their excellent spectral overlap and proximity between the donor and acceptors. The optimized ternary system (TPE-1/EY/TPE-Se) with a ratio of 1000:90:60 afforded a high energy transfer efficiency (Φ_{ET}) of 95%. Then, the artificial LHS platform catalyzed the oxidative coupling of benzylamines with 93% yield in aqueous media. Moreover, the system demonstrated broad catalytic utility oxidation reactions, the good conversion of methylthiobenzyl ester to methylbenzene sulfoxide and the aerobic cross-dehydrogenation coupling reaction of N-phenyltetrahydroisoquinoline with indole. These results robustly demonstrate the promising potential of this artificial LHS in the field of aqueous photocatalysis.

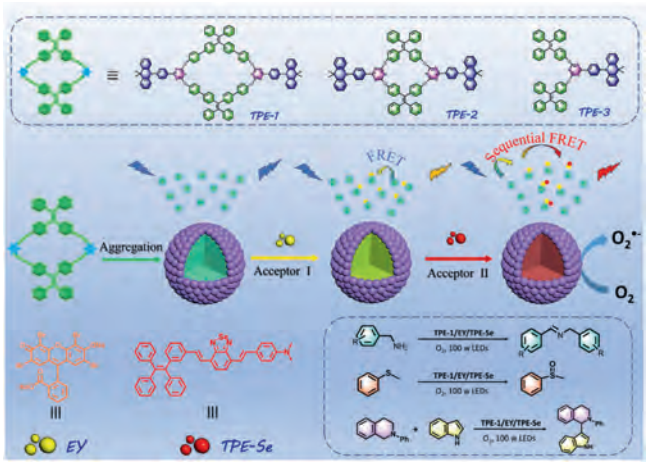
© 2026 Published by Elsevier B.V. on behalf of Chinese Chemical Society and Institute of Materia Medica, Chinese Academy of Medical Sciences.

Photosynthesis, as the essential biological solar energy conversion process on Earth, underpins the fundamental material and energy cycles sustaining life [1–5]. However, the limitation of this photocatalytic process stemming from the low energy density of single-photon absorption necessitate biomimetic approaches to artificial light-harvesting systems (ALHS) for applications spanning biological imaging [6–10], optoelectronics [11], solar energy conversion [12–14], and photocatalysis [15–22]. While early artificial LHS predominantly relied on Förster resonance energy transfer (FRET) processes mediated by covalent architectures in organic phases, contemporary research has shifted toward aqueous-phase supramolecular assemblies [23–28]. These non-covalent systems, characterized by dynamic tunability and precise donor-acceptor stoichiometric control, offer distinct advantages for mimicking natural photosynthesis [29–32]. Supramolecular complexes with aggregation-induced emission (AIE) properties are particularly promising LHS platforms due to their enhanced emissive behavior in aggregated states [33–40]. Nevertheless, most of the reported AIE-based artificial light harvesting systems predominantly emulate single-step energy transfer [41–46], failing to recapitulate the multi-step cascade energy transduction inherent to natural photosynthetic systems [47,48]. Thus, the development of sequential energy transfer architectures remains a critical unmet challenge in the field.

Recent advances in artificial LHS design have leveraged diverse platforms, including supramolecular self-assemblies, conjugated polymers, nanocrystalline arrays, dendrimers, and coordination frameworks [49–52]. Among these, supramolecular assemblies stand out for their synthetic accessibility, solution processability, and tunable photophysical properties, driving widespread adoption

* Corresponding authors.
E-mail addresses: lxsuxiaolong@126.com (X.-L. Su), tangbenz@cuhk.edu.cn (B.Z. Tang), haitaofeng907@163.com (H.-T. Feng).

https://doi.org/10.1016/j.cclet.2025.111516
1001-8417/© 2026 Published by Elsevier B.V. on behalf of Chinese Chemical Society and Institute of Materia Medica, Chinese Academy of Medical Sciences.



Scheme 1. Schematic diagram of the energy transfer process and photooxidation reaction based on TPE-1, TPE-2 and TPE-3.

in LHS construction [53–55]. These artificial LHS always shows high donor-acceptor ratio and energy transfer efficiency. Notably, AIE-active system have emerged as high-performance candidates for artificial LHS over the years, exemplified by Cao *et al.*'s 2019 report on tetraphenylethylene-based dicyclophane assemblies [56]. In addition, Xing *et al.* constructed an efficient artificial LHS with two-step sequential energy transfer in aqueous solution based on the host-guest interaction between cyano-substituted *p*-phenylenevinylene derivative and water-soluble pillar[5]arene [25]. However, most of these systems only mimic the FRET process of natural systems, often neglecting the functional integration of harvested energy into photocatalytic transformations, a hallmark of natural photosynthesis. Bridging this gap requires artificial LHS capable of not only energy capture and transfer but also catalytic energy utilization for chemical energy storage. In our recent work, we also achieved efficient two-step sequential energy transfer based on the rigid macrocycle K-1 as the energy donor in LHS. This study found that LHS based on AIE-active macrocyclic K-1 showed high photocatalytic activity for cross-dehydrogenation coupling (CDC) reaction [57].

In this study, we constructed an aqueous-phase artificial LHS featuring dual-step energy transfer cascade based on tetraphenylethylene (TPE) macrocyclic scaffolds. Two novel TPE-derived macrocycles (TPE-1 and TPE-2) with various cavity sizes were synthesized *via* a streamlined protocol exhibiting AIE behaviors. Another linear derivative TPE-3 was synthesized as a control example. In aqueous media, TPE-1 can self-assemble into nanospheres that function as high-efficiency energy donors. Through hierarchical FRET assembly, this system integrated eosin Y (EY) as a relay acceptor and TPE-Se as the terminal acceptor, achieving directional energy transfer (TPE-1 → EY → TPE-Se) with exceptional quantum efficiency (Scheme 1). The optimized TPE-1/EY binary system (1000:90 molar ratio) demonstrated an energy transfer efficiency (Φ_{ET}) of up to 97.5%, surpassing TPE-2/EY (Φ_{ET} = 91%) and TPE-3/EY (Φ_{ET} = 85%). Subsequent integration of TPE-Se enabled two-step energy transfer (TPE-1/EY/TPE-Se = 1000:90:60), achieving a cumulative Φ_{ET} of 95% and an antenna effect (AE) of 2.53. Control systems (TPE-2/EY/TPE-Se: Φ_{ET} of 93%, TPE-3/EY/TPE-Se: no secondary transfer) confirmed the critical role of TPE-1′s structural topology in energy transduction. Remarkably, the TPE-1/EY/TPE-Se system exhibited superior photocatalytic performance in aqueous oxidative coupling of benzylamines (93% yield), outperforming single-step systems (TPE-1/EY: 49%; TPE-3/EY: 37%) and the TPE-2-based dual-step analogue (82%). The TPE-1/EY/TPE-Se system was further demonstrated in thioanisole oxidation to methyl phenyl sulfoxide and the aerobic CDC reaction of *N*-phenyltetrahydroisoquinoline with indole with high conversion, underscoring its broad applicability in aqueous photocatalysis.

As shown in Schemes S1–S3 (Supporting information), TPE-1, TPE-2 and TPE-3 are rationally designed and easily synthesized. With TPE as the basic skeleton, compounds **1**, **2**, **3**, **5**, **6**, **7**, **8**, **9**, **10** are synthesized according to the published literature [58–61]. All the characterization data are consistent with those in the reported literature. Then, compounds **4** and **10** underwent Suzuki coupling under $PdCl_2$(dppf) catalyst to obtain TPE-1 in a yield of 62%. Under the same reaction conditions, compounds TPE-2 and TPE-3 were obtained with a yield of 61% and 74%, respectively. All compounds were characterized by ^{1}H NMR, ^{13}C NMR and high-resolution mass spectrometry (HRMS). Detailed synthesis steps and characterizations are described in Scheme S1–S3 and Figs. S1–S19 (Supporting information).

Density functional theory (DFT) calculations were performed to fully understand the molecular structure of TPE-1 and TPE-2. All calculations are performed using the M062X functional and the def2SVP basis set, using the D.01 revision of the Gaussian 09 program. As shown in Figs. S20A and B (Supporting information), the optimized TPE-1 and TPE-2 molecules exhibit a highly distorted conformation from the top view, which facilitates aggregated emission. The distances between two TPE double bond in the TPE-1 and TPE-2 are all 7.0 Å. The distance between the triazine groups of TPE-2 is 9.3 Å, which is much smaller than 16.5 Å of TPE-1. The well-designed cavity is spacious enough to accommodate guest molecules of appropriate size to construct a host-guest assembly with multiple characteristics. In addition, the highest occupied molecular orbital (HOMO) and the lowest unoccupied molecular orbital (LUMO) distribution are depicted by DFT calculations. HOMO is mainly distributed on the acridine skeleton, while LUMO is almost completely distributed on triazine and benzene ring connected with acridine (Figs. S20C and D). Due to the strong steric hindrance, there is a large torsion angle between the benzene ring and acridine unit, resulting in almost complete separation of HOMO and LUMO. The calculated energy gap between LUMO and HOMO is 2.97 and 2.96 eV for TPE-1 and TPE-2, respectively. The lowest energy gap between the singlet and triplet states ($\Delta E_{S1\text{-}T1}$) of TPE-1 and TPE-2 were calculated to be 0.07 and 0.10 eV for (Figs. S20C and D), which accelerates intersystem crossing (ISC) to the triplet state.

The basic photophysical properties of TPE-1, TPE-2 and TPE-3 are then studied by using ultraviolet-visible (UV–vis) and photoluminescence (PL) spectra. The absorption spectra of TPE-1 and TPE-2 centered at 355 and 310 nm in THF (1×10^{-5} mol/L) (Figs. S21A and B in Supporting information). The main band of TPE-3 located at 310–400 nm. Then, the AIE behaviors of TPE-1, TPE-2 and TPE-3 in H_2O/THF mixture are evaluated by PL spectroscopy (Fig. S22 in Supporting information). Taking TPE-1 as an example, it emits weak blue-green fluorescence in pure THF solution, and the quantum yield (QY) is 6.1% (Fig. S23 in Supporting information). When the poor solvent (water) was added to the THF solution, the fluorescence intensity did not change significantly from 0 to 40% water. Further increasing the water fraction to 95% led to a significant increase in fluorescence with a quantum yield of 33.9% (Fig. S22A). At the same time, the AIE behavior of TPE-2 and TPE-3 in H_2O/THF mixture are also studied, and the fluorescence significantly enhanced when the water fraction was 90% (Figs. S22B and C). The above results show that TPE-1, TPE-2 and TPE-3 are typical AIEgens. In order to simulate natural LHS, H_2O/THF mixtures with water content of 95%, 90% and 90% were selected as the solution phase for the following experiments.

Next, we systematically investigated the one-step energy transfer processes between three AIEgens (TPE-1, TPE-2, TPE-3) and the

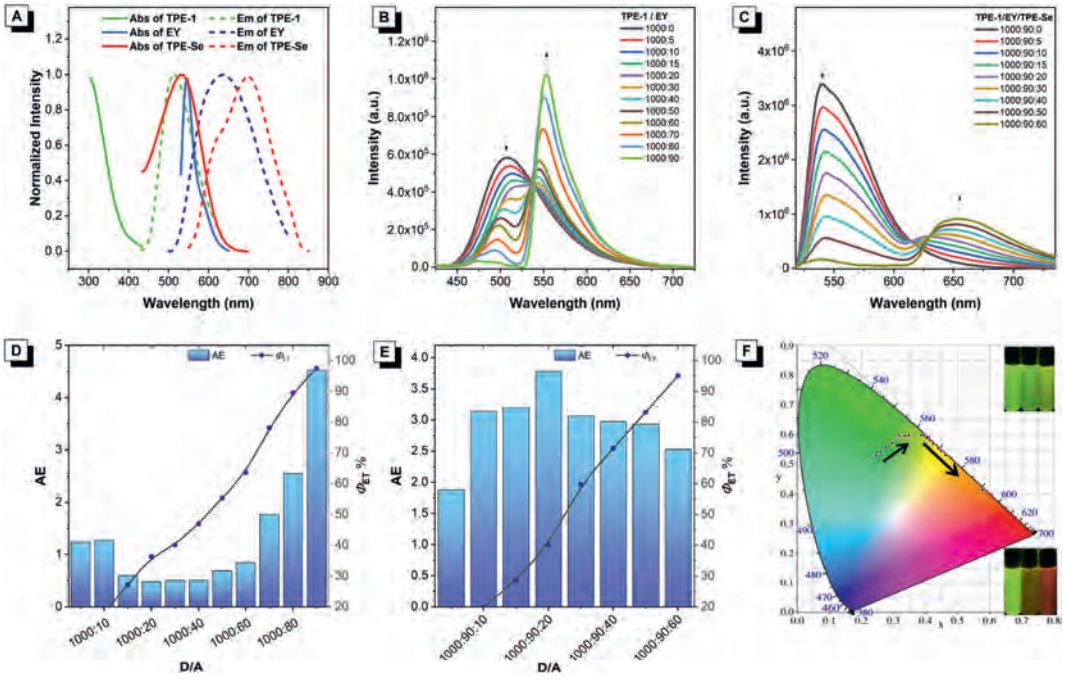


Fig. 1. (A) Normalized absorption spectra of TPE-1 (green line), EY (blue line), TPE-Se (red line) and their normalized emission spectra (dashed lines). (B) Fluorescence spectra of TPE-1 with different concentrations of EY. λ_{ex} = 355 nm, E_x/E_m slit = 1/1 nm. (C) Fluorescence spectra of TPE-1/EY (1000:90) with different concentrations of TPE-Se. λ_{ex} = 355 nm, E_x/E_m slit = 1/1 nm. Energy transfer efficiency and AE at (D) different TPE-1/EY ratios, (E) different TPE-1/EY/TPE-Se ratios. (F) Commission International de L'Elairage (CIE) 1931 chromaticity coordinates changes of (B) and (C). Inset: the fluorescence photos of TPE-1, TPE-1/EY and TPE-1/EY/TPE-Se suspension.

energy acceptor EY. Next, we systematically investigated the one-step energy transfer processes between three AIEgens (TPE-1, TPE-2, TPE-3) and the energy acceptor EY. As illustrated in Fig. 1A, the emission spectrum of TPE-1 exhibits significant spectral overlap with the absorption profile of EY, establishing EY as the optimal acceptor. Upon incremental addition of EY to the TPE-1 solution under 355 nm excitation, the fluorescence intensity of EY at 551 nm progressively intensified, concomitant with a marked attenuation of TPE-1 emission at 501 nm (Fig. 1B). This spectral evolution was visually corroborated by a distinct chromatic shift from blue-green to yellow-green (Fig. 1F). Control experiments conducted at EY's intrinsic excitation wavelength (501 nm) revealed fluorescence enhancement (Fig. S24A in Supporting information), whereas direct excitation of EY at 355 nm generated negligible emission due to its inherent aggregation-caused quenching (ACQ) properties (Fig. S24B in Supporting information), thereby confirming energy transfer rather than direct excitation artifacts. Quantitative analysis of the LHS performance was conducted through energy transfer efficiency and AE calculations (Table S1). At a donor-acceptor ratio of 1000:5 in H_2O/THF (19/1, v/v), Φ_{ET} was 9.1 % with AE = 1.24 (Fig. 1D). By increasing the EY content to 1000:90, the Φ_{ET} was increased to 97.5 %, and the AE was significantly enhanced to 4.20, suggesting enhanced FRET efficiency through optimized molecular accommodation within TPE-1 cavities. Then, the time-resolved fluorescence decay curve was performed to further verify the energy transfer process. The average lifetime of TPE-1 in H_2O/THF (19/1, v/v) was 19.76 ns. When assembled with EY, the lifetime of TPE-1/EY (1000:30, 1000:60, 1000:90) aggregates decreased to 14.11, 10.66, 1.63 ns, respectively (Fig. S25A in Supporting information), indicating the efficient energy transfer efficiency of TPE-1 to the acceptor EY. Similar energy transfer processes were observed in TPE-2/EY and TPE-3/EY systems. For TPE-2, spectral overlap between its absorption and EY emission facilitated energy transfer under 310 nm excitation (Fig. 2A). Progressive EY addition induced fluorescence enhancement at 547 nm (EY's emission) with concurrent donor emission (519 nm) suppression (Fig. 2B), accompanied by analogous chromatic shifts (Fig. 2F). Control experiments at EY's excitation wavelength (519 nm) demonstrated fluorescence amplification (Fig. S24E in Supporting information), while direct EY excitation at 310 nm yielded minimal emission (Fig. S24F in Supporting information), excluding trivial excitation artifacts. The performance of LHS was quantitatively evaluated by measuring the energy transfer efficiency and AE with different proportions of EY (Table S3 in Supporting information). The Φ_{ET} value was calculated to be 10.6 % at a ratio of 1000:4 in 90 % water fraction, and the AE value was determined to be 0.03 (Fig. 2D), which improved to Φ_{ET} = 91 % and AE = 1.83 at 1000:30 (Fig. 2D, Table S3). The average lifetime of TPE-2 in H_2O/THF (9/1, v/v) decreased from 19.73 to 16.46 ns (1000:10), 15.15 ns (1000:20), and 6.32 ns (1000:30) upon assembly with EY (Fig. S25C in Supporting information). Moreover, TPE-3 can also be used as donors to occur energy transfer process with and EY (Fig. S26 in Supporting information). The TPE-3/EY (1000:30) achieved Φ_{ET} = 84.9 % and AE = 102.5 (Fig. S26). Notably, macrocyclic TPE-1 and TPE-2 outperformed linear TPE-3 in energy transfer metrics.

To expand the spectral range, we engineered a two-step artificial LHS (AIEgens/EY/TPE-Se) in aqueous media. This design leverages the substantial spectral overlap between EY's fluorescence emission (λ_{em} = 545 nm) and TPE-Se's absorption band, establishing AIEgens as primary donors, EY as relay acceptors, and TPE-Se as terminal acceptors (Figs. 1A and 2A). Upon introducing TPE-Se into the TPE-1/EY system, we observed an obvious fluorescence enhancement at 670 nm (TPE-Se) accompanied by significant quenching of EY emission at 545 nm (Fig. 1C). The optimized TPE-1/EY/TPE-Se assembly (1000:90:60 molar ratio) achieved exceptional energy transfer efficiency (95 %) with an AE value of 2.53, accompanied by a distinct emission color shift from yellow-green to red (Figs. 1E and F, Table S2 in Supporting information). In the control experiment, the aggregates of TPE-1/EY (1000:90) were titrated with TPE-Se (excitation at 545 nm), and the fluorescence intensity was weaker than that under 310 nm excitation (Fig. S24C in Supporting information), direct excitation of TPE-Se

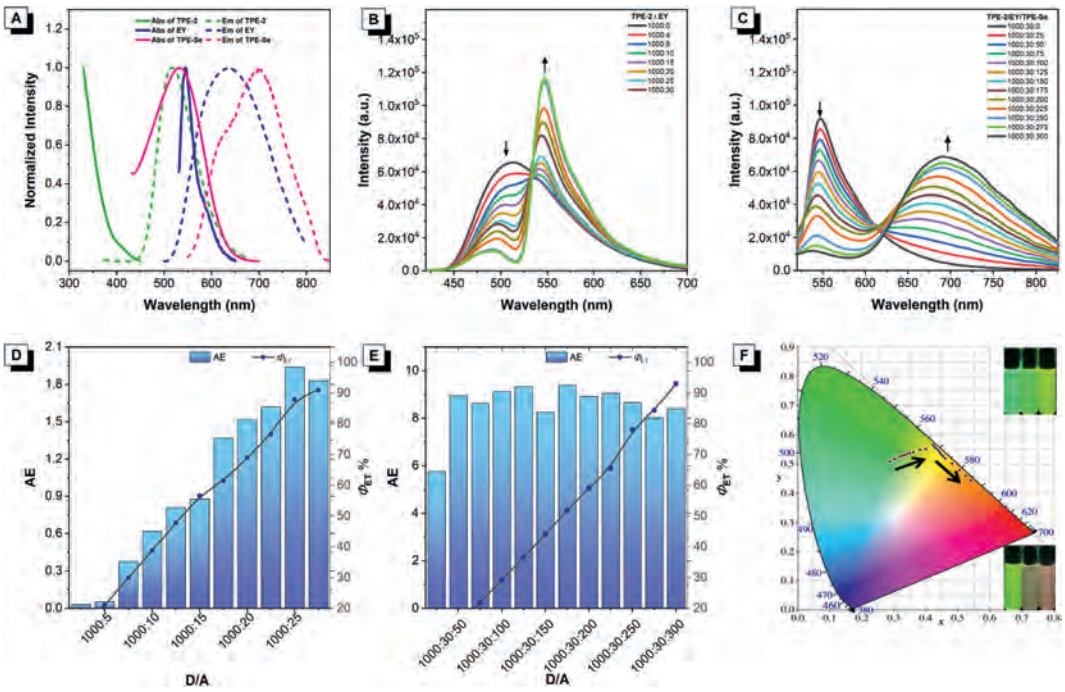


Fig. 2. (A) Normalized absorption spectra of TPE-2 (green line), EY (blue line), TPE-Se (red line) and their normalized emission spectra (dashed lines). (B) Fluorescence spectra of TPE-2 with different concentrations of EY. $\lambda_{ex} = 310$ nm, E_x/E_m slit = 1/1 nm. (C) Fluorescence spectra of TPE-2/EY (1000:30) with different concentrations of TPE-Se. $\lambda_{ex} = 310$ nm, E_x/E_m slit = 1/1 nm. Energy transfer efficiency and AE at (D) different TPE-2/EY ratios, (E) different TPE-2/EY/TPE-Se ratios. (F) CIE 1931 chromaticity coordinates changes of (B) and (C). Inset: the fluorescence photos of TPE-2, TPE-2/EY and TPE-2/EY/TPE-Se suspension.

at 355 nm produced negligible emission (Fig. S24D in Supporting information), which excluded the possibility that the energy at 545 nm was not directly excited by TPE-Se under 310 nm excitation. The time-resolved fluorescence decay curves of TPE-1/EY/TPE-Se (1000:90:30, 1000:90:60) showed that the lifetime decreased from 3.57 ns (1000:30:0) to 1.43 and 1.39 ns (Fig. S25B in Supporting information), which also proved the occurrence of energy transfer. Similar energy transfer cascades were established in TPE-2/EY systems through TPE-Se titration. Fluorescence monitoring revealed progressive intensity enhancement at 689 nm (TPE-Se) with concomitant reduction at 550 nm (EY) (Fig. 2C). The TPE-2/EY/TPE-Se assembly (1000:30:300) demonstrated 93% energy transfer efficiency (Φ_{ET}) and AE = 2.53, accompanied by analogous yellow-green-to-red emission shifts (Figs. 2E and F, Table S4 in Supporting information). Through the DLS and SEM characterization of the FRET system, it was found that the morphology and particle size changed significantly, and the energy transfer process was also confirmed (Fig. S27 in Supporting information). Comparative analysis highlighted that TPE-1′s superior energy transfer performance over TPE-2 counterparts, with TPE-3′s system showing no secondary energy transfer, confirming the critical role of macrocyclic architecture in constructing efficient aqueous FRET-based LHS.

To better emulate natural photosynthesis and optimize energy utilization, the TPE-1/EY/TPE-Se ternary system (1000:90:60 molar ratio) served as an efficient photocatalyst for aqueous-phase oxidative coupling of benzylamine to imine under 100 W blue light-emitting diodes (LEDs) illumination (Fig. S28 in Supporting information). We used 100 W blue LEDs as a simulated light source for the reaction. No product formation occurred in control experiments without catalyst (Table S6 in Supporting information, entry 1) or under dark conditions (Table S6, entry 2). Isolated fluorophores TPE-1, TPE-2, TPE-3, EY, and TPE-Se exhibited moderate photocatalytic activity with yields of 44%, 27%, 21%, 39%, and 14%, respectively (Table S6, entries 3–7). Under the same conditions, combinations including TPE-1+EY, TPE-2+EY, TPE-3+EY, TPE-1+TPE-Se, TPE-2+TPE-Se, TPE-3+TPE-Se and EY+TPE-Se achieved yields ranging from 26% to 49% (Table S6, entries 8–14). The TPE-1/EY/TPE-Se assembly demonstrated exceptional catalytic efficiency (93% yield), substantially outperforming TPE-2 (82%) and TPE-3 (61%) counterparts (Table S6, entries 15–17), validating its enhanced FRET-driven photocatalytic capability. When using TPE-1 ternary component as catalyst, changing its equivalent, 2 mol% provided optimal performance (Table S7 in Supporting information); Subsequently, under 100 W blue light achieved optimal conversion (Table S8 in Supporting information). The control experiment confirmed the critical oxygen dependence: the reaction yield decreased to 74% in air, but reached 93% in O_2, and no reaction occurred in N_2 (Tables S9–S11 in Supporting information). Therefore, the optimal reaction conditions were established: benzylamine (1 mmol), TPE-1+EY+TPE-Se assembly solution (2 mol%), H_2O/THF = 19/1, 100 W blue LEDs, room temperature, 12 h (Table S6, entry 15).

Under the optimized reaction conditions, we systematically investigated the substrate scope using diverse benzylamine derivatives. As summarized in Fig. 3, both electron-withdrawing and electron-donating substituted benzylamine derivatives underwent efficient conversion under these conditions, delivering corresponding products **2a**–**2f** in excellent yields ranging from 88% to 95%. Notably, the disubstituted substrate also demonstrated good reactivity, achieving an 89% yield for product **2g**. Particularly it was noteworthy that the 95% yield obtained when employing 2-thiophenemethylamine (**2h**), indicating remarkable compatibility with heteroaromatic systems. The catalytic system exhibited exceptional versatility, successfully accommodating dibenzylamine (**2i**, 95%) and extending to 1,2,3,4-tetrahydroisoquinoline and 2-phenylimidazoline (**2j**–**2k**, 78%–92%). Beyond amine substrates, this methodology proved effective for sulfur-containing compounds, as evidenced by the oxidation of thioanisole to methyl phenyl sulfoxide in 81% yield (Scheme S4A in Supporting information), and the aerobic CDC reaction of

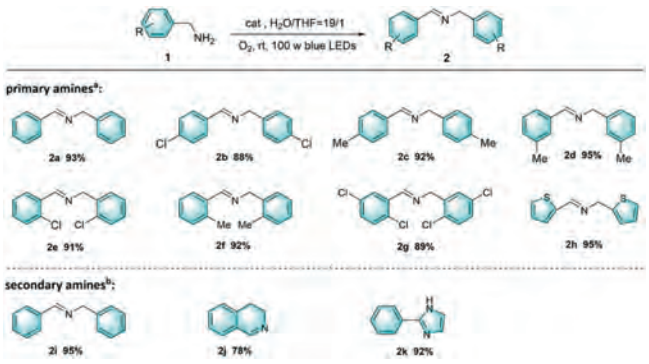


Fig. 3. The benzylamine coupling of primary amines to imines by TPE-1/EY/TPE-Se. [a]Substrate (1.0 mmol) were dissolved in the freshly prepared TPE-1+EY+TPE-Se assembly solution (2 mol%). [b]Substrate (1.0 mmol) were dissolved in the freshly prepared TPE-1+EY+TPE-Se assembly solution (1 mol%). [c]Isolated yields.

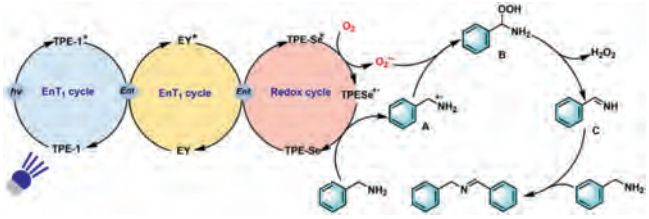


Fig. 4. A plausible mechanism for the benzylamine photocatalysis reaction using TPE-1/EY/TPE-Se nanoparticles as a photocatalyst in aqueous medium.

N-phenyltetrahydroisoquinoline with indole in 79 % yield (Scheme S4B in Supporting information). All products were unambiguously characterized by comprehensive ^{1}H and ^{13}C NMR analyses (Figs. S29–S54 in Supporting information). The excellent catalytic ability of the TPE-1/EY/TPE-Se (1000:90:60) module in various substrates was demonstrated. This rationally designed ternary system represents a robust photocatalytic platform capable of converting solar energy into chemical energy in aqueous media, showcasing significant potential for sustainable chemical synthesis.

To elucidate the photocatalytic mechanism governing the oxidative coupling of benzylamine derivatives, we conducted systematic radical trapping experiments using established scavengers:2,2,6,6-tetramethylpiperidine oxide (TEMPO), butylated hydroxytoluene (BHT), 1,4-benzoquinone, potassium iodide (KI), isopropanol, β-carotene and catalase. These scavengers are used to capture all photogenerated free radicals, such as $O_2^{\bullet-}$, holes (h^+), hydroxyl radicals ($^{\bullet}OH$), $^{1}O_2$ and H_2O_2. This method enables us to study the mechanisms and active substances involved in the reaction. As shown in Table S12 (Supporting information), the reaction exhibited distinct scavenger-dependent behavior. Complete inhibition of benzylamine photooxidation occurred with TEMPO or BHT addition. After the introduction of benzoquinone, the photooxidation reaction yield of benzylamine was significantly suppressed. Addition of KI reduced the yield of the reaction likely due to the electronic effect. Negligible effects were recorded for systems containing isopropanol, β-carotene, or catalase. This mechanistic profile conclusively identifies superoxide radicals ($O_2^{\bullet-}$) as the predominant reactive species driving the oxidative coupling process. The differential inhibition patterns further suggest synergistic interplay between multiple active intermediates in the photocatalytic cycle.

Based on mechanistic insights from our experimental findings and supported by previous studies [62–71], we propose a cascade energy transfer-driven photocatalytic mechanism for benzylamine oxidative coupling (Fig. 4). The rationally designed TPE-1/EY/TPE-Se ternary system establishes a FRET-mediated excitation cascade. Blue light irradiation induces TPE-1 excitation, followed by directional energy transfer to [EY]* and subsequently to TPE-Se, resulting in the production of [TPE-Se]*. The accumulated energy in [TPE-Se]* drives direct electron transfer to molecular oxygen, generating critical superoxide radicals ($O_2^{\bullet-}$) and forming $[TPE\text{-}Se]^{+\bullet}$. Then, $[TPE\text{-}Se]^{+\bullet}$ oxidizes benzylamine *via* single-electron transfer, yielding radical cation Intermediate **A**. Subsequently, $O_2^{\bullet-}$ extracted a proton from the benzylamine radical cation to produce intermediate **B**. Spontaneous H_2O_2 elimination generates Intermediate **C**. Finally, the intermediate **C** reacts with the new benzylamine molecule through nucleophilic attack to products.

In summary, we have engineered an innovative ALHS leveraging the AIE characteristics of macrocyclic tetraphenylethylene derivative TPE-1, which enables sequential FRET in aqueous media. As an ideal energy donor, TPE-1 facilitated the one step of energy transfer upon the introduction of EY as the energy acceptor. Subsequently, EY as a relay donor transferred its energy to the final energy acceptor TPE-Se, thus a two-step energy transfer process was successfully achieved. Compared to the TPE-2 with a smaller cavity and the non-cyclic molecule TPE-3, the ALHS based on the macrocyclic structure TPE-1 possessing a larger cavity exhibited significantly higher energy transfer efficiency. The calculated energy transfer efficiencies for the TPE-1/EY system and the TPE-1/EY/TPE-Se system were 97.5 % and 95 %, respectively. Furthermore, the energy harvested by the TPE-1/EY/TPE-Se system could not only be utilized for the oxidative coupling of benzylamine and its derivatives in an aqueous medium but also catalyze the oxidation of thioanisole to produce methyl phenyl sulfoxide and the aerobic CDC reaction of *N*-phenyltetrahydroisoquinoline with indole. This study provides valuable insights into the application of sequential energy transfer-based ALHS in aqueous photocatalytic chemical reactions.

Declaration of competing interest

The authors declare that they have no known competing financial interests or personal relationships that could have appeared to influence the work reported in this paper.

CRediT authorship contribution statement

Meng-Xin Liu: Writing – original draft, Software, Methodology, Investigation. **Xiao-Long Su:** Writing – review & editing, Writing – original draft, Supervision, Software, Funding acquisition, Formal analysis. **Pu Chen:** Software, Methodology. **Yan-Yan Liu:** Software, Methodology. **Jian-Peng Li:** Investigation, Formal analysis. **Li Zou:** Software, Formal analysis, Data curation. **Ben Zhong Tang:** Writing – review & editing, Supervision, Project administration, Methodology. **Hai-Tao Feng:** Writing – review & editing, Writing – original draft, Project administration, Funding acquisition.

Acknowledgments

This work was supported by the National Natural Science Foundation of China (No. 52173152), the Fund of the Rising Stars of Shaanxi Province (No. 2021KJXX-48), Scientific and Technological Innovation Team of Shaanxi Province (No. 2022TD-36), The Natural Science Basic Research Plan in Shaanxi Province of China (No. 2024JC-YBMS-123) and Industrial Science and Technology Plan in Shaanxi Provincial Education Department (No. 23JC001).

Supplementary materials

Supplementary material associated with this article can be found, in the online version, at doi:10.1016/j.cclet.2025.111516.

References

[1] L. Zhou, Y. Zhou, L. Fang, et al., Chin. Chem. Lett. 35 (2024) 109509.
[2] W. Zhang, Y. Luo, X.L. Ni, Z. Tao, X. Xiao, Chem. Eng. J. 446 (2022) 136954.
[3] D. Zhang, W. Yu, S. Li, et al., Chem. Soc. 143 (2021) 1313–1317.
[4] X.Q. Xu, Y.R. Song, J.H. Cao, et al., Chem. Sci. 16 (2025) 5786–5796.
[5] T. Xiao, H. Wu, G. Sun, et al., Chem. Commun. 56 (2020) 12021–12024.
[6] L. Xu, Coord. Chem. Rev. 506 (2024) 215726.
[7] X. Tian, S. Li, K. Velmurugan, et al., Mater. Chem. Front. 7 (2023) 2484–2492.
[8] Z. Liu, X. Sun, X. Dai, et al., J. Mater. Chem. C 9 (2021) 1958–1965.
[9] Y.X. Hu, W.J. Li, P.P. Jia, et al., Adv. Opt. Mater. 8 (2020) 5250–5257.
[10] X.M. Chen, Q. Cao, H.K. Bisoyi, et al., Angew. Chem. Int. Ed. 59 (2020) 10493–10497.
[11] W. Zhang, C. Kuang, X. Chen, X. Yang, H. Guan, Appl. Surf. Sci. 566 (2021) 150652.
[12] M.K. Panda, K. Ladomenou, A.G. Coutsolelos, Coord. Chem. Rev. 256 (2012) 2601–2627.
[13] M.E. El-Khouly, E. El-Mohsnawy, S. Fukuzumi, J. Photochem. Photobiol. C 31 (2017) 36–83.
[14] H.X. Liu, D.H. Si, M.F. Smith, et al., Aggregate 4 (2023) e383.
[15] F. Xiang, D. Wang, K. Xu, C.C. Zeng, Org. Lett. 26 (2023) 411–415.
[16] N.A. Romero, D.A. Nicewicz, Chem. Rev. 116 (2016) 10075–10166.
[17] Y. Pan, S. Wang, C.W. Kee, et al., Green Chem. 13 (2011) 3341–3344.
[18] A.U. Meyer, K. Straková, T. Slanina, B. König, Chem. Eur. J. 22 (2016) 8694–8699.
[19] Y. Meng, C. Pan, N. Liu, et al., Green Chem. 26 (2024) 300–305.
[20] C.Q. Ma, N. Han, Y. Wang, et al., Dyes Pigm 211 (2023) 111076.
[21] M.H. Huang, Y.L. Zhu, W.J. Hao, et al., Adv. Synth. Catal. 359 (2017) 2229–2234.
[22] A.L. Fuentes de Arriba, F. Urbitsch, D.J. Dixon, Chem. Commun. 52 (2016) 14434–14437.
[23] T.X. Xiao, X.X. Li, L.L. Zhang, et al., Chin. Chem. Lett. 35 (2024) 108618.
[24] T. Xiao, H. Qian, X. Li, et al., Dyes Pigm. 215 (2023) 111289.
[25] Y. Wang, N. Han, X.L. Li, R.Z. Wang, L.B. Xing, ACS Appl. Mater. Interfaces 14 (2022) 45734–45741.
[26] G. Sun, M. Li, L. Cai, et al., Chem. Commun. 60 (2024) 1412–1415.
[27] Q. Song, S. Goia, J. Yang, et al., J. Am. Chem. Soc. 143 (2020) 382–389.
[28] Y.S. Bi, R.Z. Zhang, K.K. Niu, et al., Chin. Chem. Lett. 36 (2025) 110311.
[29] X. Li, S. Yu, Z. Shen, et al., J. Colloid Interface Sci. 617 (2022) 118–128.
[30] J.J. Li, H.Y. Zhang, X.Y. Dai, Z.X. Liu, Y. Liu, Chem. Commun. 56 (2020) 5949–5952.
[31] G.L. Li, K.K. Niu, X.Z. Yang, et al., J. Mater. Chem. A 12 (2024) 13356–13363.
[32] S. Garain, B.C. Garain, M. Eswaramoorthy, S.K. Pati, S.J. George, Angew. Chem. Int. Ed. 60 (2021) 19720–19724.
[33] H.T. Feng, Y. Li, X. Duan, et al., J. Am. Chem. Soc. 142 (2020) 15966–15974.
[34] H.T. Feng, S.M. Zou, M. Chen, et al., J. Am. Chem. Soc. 142 (2020) 11442–11450.
[35] X.X. Wang, S. Xiang, C.X. Qi, et al., ACS Nano 16 (2022) 8223–8232.
[36] X. Tang, Y. Zhu, W. Guan, C. Lu, Aggregate 4 (2023) e348.
[37] X.L. Su, J.P. Li, M.X. Liu, et al., Chin. J. Org. Chem. 44 (2024) 2581–2587.
[38] S. Xiang, P.P. Lv, C.S. Guo, et al., Chem. Commun. 57 (2021) 13321–13324.
[39] P. Chen, J.W. Zhao, D. Li, et al., Coord. Chem. Rev. 533 (2025) 216548.
[40] X.L. Su, L. Zou, J.P. Li, et al., Dyes Pigm. 241 (2025) 112877.
[41] T. Xiao, X. Wei, H. Wu, et al., Dyes Pigm. 188 (2021) 109161.
[42] K. Wang, Y. Shen, P. Jeyakkumar, et al., Curr. Opin. Green Sustain. Chem. 41 (2023) 100823.
[43] Z. Lian, M. Jiang, F. Qiao, et al., J. Photochem. Photobiol. A 386 (2020) 112135.
[44] H.T. Feng, X. Zheng, X. Gu, et al., Chem. Mater. 30 (2018) 1285–1290.
[45] K. Acharyya, S. Bhattacharyya, H. Sepehrpour, et al., J. Am. Chem. Soc. 141 (2019) 14565–14569.
[46] X.L. Li, D.L. Cheng, K.K. Niu, et al., J. Mater. Chem. A 11 (2023) 24911–24917.
[47] T. Matsuo, K. Ikeda, S. Hayashi, Aggregate 4 (2023) eabn9057.
[48] W.C. Yang, S.Y. Li, S. Ni, G. Liu, Aggregate 5 (2023) e460.
[49] H.T. Feng, W.Y.Jacky Lam, B.Z. Tang, Coord. Chem. Rev. 406 (2020) 213142.
[50] P.P. Jia, L. Hu, W.T. Dou, et al., J. Mater. Chem. C 11 (2023) 6607–6615.
[51] X.L. Li, S. Yu, M.N. Chen, et al., J. Photochem. Photobiol. A 410 (2021) 113182.
[52] K.X. Teng, Z.P. An, L.Y. Niu, Q.Z. Yang, ACS Mater. Lett. 6 (2023) 290–297.
[53] Z. Wu, H. Qian, X. Li, T. Xiao, L. Wang, Chin. Chem. Lett. 35 (2024) 108829.
[54] Y. Xia, M. Chen, S. Li, et al., J. Mater. Chem. C 10 (2022) 12332–12337.
[55] R.Z. Zhang, H. Liu, C.L. Xin, et al., J. Colloid Interface Sci. 651 (2023) 894–901.
[56] Y.D. Li, L. Cheng, C.Y. Qin, et al., J. Am. Chem. Soc. 11 (2019) 12288–12305.
[57] J.C. Yang, K. Chen, G.L. Zhang, et al., Chem. Sci. 16 (2025) 4741–4748.
[58] F.Y. Ye, J.H. Chen, S.H. Liu, Org. Lett. 6 (2019) 3950–3955.
[59] J. Luo, Y.F. Ao, Q.Q. Wang, D.X. Wang, Angew. Chem. Int. Ed. 57 (2018) 15827–15831.
[60] W.L. Zhao, Y.F. Wang, S.P. Wan, et al., CCS Chem. 4 (2022) 3540–3548.
[61] Z. Wang, X.W. He, T.Y. Yong, et al., J. Am. Chem. Soc. 27 (2020) e202400388.
[62] J. Kou, G. Wang, H. Guo, et al., Appl. Catal. B 352 (2024) 124020.
[63] X. Lang, H. Ji, C. Chen, W. Ma, J. Zhao, Angew. Chem. Int. Ed. 50 (2011) 3934–3937.
[64] F. Su, S.C. Mathew, L. Möhlmann, et al., Angew. Chem. Int. Ed. 50 (2011) 657–660.
[65] J.D. Tibbetts, D.R. Carbery, E.A.C. Emanuelsson, ACS Sustain. Chem. Eng. 5 (2017) 9826–9835.
[66] Y. Liu, K. Ji, J. Wang, et al., ACS Appl. Mater. Interfaces 14 (2022) 27882–27890.
[67] Q. Niu, Q. Huang, T.Y. Yu, et al., J. Am. Chem. Soc. 144 (2022) 18586–18594.
[68] W. Phasayavan, M. Japa, S. Pornsuwan, et al., J. Colloid Interface Sci. 581 (2021) 719–728.
[69] M.Y. Yang, S.B. Zhang, M. Zhang, et al., J. Am. Chem. Soc. 146 (2024) 3396–3404.
[70] R.Z. Zhang, K.K. Niu, Y.S. Bi, et al., Small 21 (2025) 2405564.
[71] L.B. Xing, K. Cheng, H. Li, et al., Angew. Chem. Int. Ed. 64 (2025) e202425668.